Towards a better understanding of the high-temperature oxidation of MAX phase Cr2AlC

A. Zuber, V. Gauthier-Brunet, J. Roger, J. Gonzalez-Julian, T. Ouisse, Sylvain Dubois

Journal of the European Ceramic Society 42 (2022) 2089–2096

Contents lists available at ScienceDirect

Journal of the European Ceramic Society

journal homepage: www.elsevier.com/locate/jeurceramsoc

Towards a better understanding of the high-temperature oxidation of MAX phase Cr_2AlC

A. Zuber [a,*], V. Gauthier-Brunet [a], J. Roger [b], J. Gonzalez-Julian [c], T. Ouisse [d], S. Dubois [a]

[a] Institut PPRIME, CNRS/Université de Poitiers/ENSMA, UPR 3346, TSA 41126, 86073, Poitiers Cedex 9, France
[b] Université de Bordeaux, CNRS, Laboratoire des Composites ThermoStructuraux, UMR 5801, 33600, Pessac, France
[c] Chair of Ceramics, Institute of Mineral Engineering (GHI), RWTH Aachen University, Forckenbeckstrasse 33, 52074, Aachen, Germany
[d] Université Grenoble-Alpes, CNRS, Grenoble INP, LMGP, 38000, Grenoble, France

ARTICLE INFO

Keywords:
Cr_2AlC
High-temperature oxidation
Microstructure
Single crystal
Thermodynamic calculations

ABSTRACT

High-temperature oxidation of bulk single crystal, fine and coarse grained polycrystals of Cr_2AlC has been performed from 800 °C to 1500 °C. In the temperature range T = [800;1400] °C, an α-Al_2O_3 scale with a Cr_7C_3 subscale are *in-situ* formed independently of the initial microstructure on top of the bulk Cr_2AlC. CALPHAD calculations were performed to explain the formation of Cr_7C_3 instead of the expected mixture of carbides, indicating a favourable driving force for Cr_7C_3 formation. The kinetic study of the oxidation is consistent with previous works with an activation energy of about 400 kJ.mol^{-1}. Oxidizing for a longer time (1000 h) or at higher temperature (1500 °C) leads to the formation of chromia in the former alumina scale, which correspond to the calculated equilibrium phases.

1. Introduction

MAX phases are a family of nanolayered carbides and nitrides with formula $M_{n+1}AX_n$ (n = 1, 2, 3) discovered in late 70′s and widely studied since the early 2000′s for their unique properties cumulating those of ceramics and metals [1,2]. The oxidation behaviour of these materials has been studied since 2005, Cr_2AlC being considered as one of the most promising MAX phase for its corrosion resistance properties [3]. Oxidation of bulk Cr_2AlC has been studied from 700 °C to 1400 °C for various oxidation times [4–11], the most common observation being the formation of a continuous layer of α -Al_2O_3. This α-Al_2O_3 layer is often observed with θ-Al_2O_3 on top, as it is often reported on top of NiAl alloys [9,12].

Depending on the work considered, several other features were pointed out like spallation and cracking of the oxide scale, the existence of a chromium traces or a chromia-rich region in the oxide scale, the formation of a Cr_7C_3 sublayer or pores in such a layer. The occurrence, in literature, of these observations is reported in Table 1.

The pore formation in the carbide sublayer is explained by carbon and chromium oxides evaporation [4,8]. Nevertheless, only carbon dioxide has been detected in the early work of Lin et al. [5].

Some observations were scarcer and often proper to Cr_2AlC films like formation of Cr_3C_2 or chromium in the oxide scale. Hajas et al. [13] reported small blistering of the oxide scale and the formation of both Cr_7C_3 and Cr_3C_2 under the alumina scale, the latter being a common observation with the works of Wang et al. [14]. Overall, the early studies on the oxidation of Cr_2AlC concluded on the good oxidation resistance of the oxide scale up to 1200 °C and a deterioration of its properties above. The species observed after the oxidation process seem to be the same for all studied temperatures.

The studies of the microstructure's influence on the oxidation behaviour of Cr_2AlC focused on the grain size effect: Li et al. observed the formation of a Cr_7C_3 subscale under the alumina scale of coarse grained (60 μm) samples after 2 h oxidation at 1100 °C while they did not observe any in the case of fine grained (2 μm) samples. Moreover, they did not find any carbide after oxidation times up to 100 h for both fine and coarse-grained samples [11]. This study is the only one to our knowledge about the microstructure influence on the oxidation of dense bulk Cr_2AlC.

Kinetic studies mainly pointed out the parabolic behaviour of aluminum-based MAX-phases [5,8]. Tallman et al. [3] demonstrated the inaccuracy of using parabolic law and promoted power law as a more accurate way to investigate the oxidation behaviour of MAX-phases. The main argument for this method is that the kinetics often tend to be cubic and yield to activation energy of about 350−400 kJ.mol^{-1}. Such an energy corresponds to the activation energy for oxygen diffusion at the

* Corresponding author.
E-mail address: axel.zuber@univ-poitiers.fr (A. Zuber).

https://doi.org/10.1016/j.jeurceramsoc.2021.12.057
Received 30 November 2021; Received in revised form 18 December 2021; Accepted 21 December 2021
Available online 24 December 2021

grain boundaries of the alumina scale [15]. The formation of the oxide scale is therefore quite well understood whereas the presence of the carbide sublayer is simply described as the result of aluminum depletion in the MAX phase. Using CALPHAD thermodynamic calculations, Hajas et al. concluded that the oxidation of Cr_2AlC leads to the formation of a Cr_7C_3 layer partly because of the oxidation of Cr_3C_2 but the explanation remains unclear. Indeed, phase diagrams evidence the presence of both species Cr_7C_3 and Cr_3C_2 when considering the stable phases with Cr_2C composition [16].

The present paper focuses on the oxidation behaviour of bulk Cr_2AlC in dry air in the temperature range 800−1500 °C up to 1000 h, in relation with the microstructure. The objective is to clarify the influence of grain size, grain orientation and surface roughness on the oxidation of Cr_2AlC. For that purpose, oxidation products are characterized and oxidation kinetics of single crystals as well as coarse and fine grained polycrystals are compared. Influence of surface roughness on the oxidation process is also investigated in the case of the short-time oxidation of single crystal samples. Thermodynamic calculations are performed to better understand the nature of both the carbide sublayer and the different phases formed during the oxidation.

2. Method

2.1. Synthesis method

For coarse grained sample synthesis, high purity 350+ mesh powders of chromium (Alfa Aesar, purity >99 %), aluminum (Alfa Aesar, purity >995%) and chromium carbide (Alfa Aesar, purity >995%) were mixed with a molar ratio $Cr:Cr_3C_2:Al = 0.525:0.475:1.2$ in a tridimensional Turbula® mixer for 10 min. The powder mixture was then uniaxially cold-pressed (35 MPa) into a cylindrical green pellet (12 mm diameter). The pellet was encapsulated into a glass container under primary vacuum to prevent oxidation during the subsequent heat treatment. An isostatic Ar pressure of 150 MPa was thus applied at 1400 °C during 4 h using a Hot Isostatic Press (ACB-HIP6). The pressure was maintained while cooling. Surfaces of the samples were ground to eliminate glass-induced pollution.

For fine grained sample synthesis, chromium (Alfa Aesar, purity: 99 %, d50: 28.0 μm), aluminum (Alfa Aesar, purity: 99.5 %, D50 = 9.1 μm) and graphite (Alfa Aesar, purity 99.0 %, D50 = 6.9 μm) powders were mixed with a molar ratio $Cr_2Al_{1.02}C_{0.97}$ using a planetary milling. The mixture was milled using 5 mm diameter ZrO_2 milling balls in a powder/ball ratio of 1:1 during 24 h in ethanol. Afterwards, the milling balls were removed, and the powder was dried in a rotary evaporator and in an oven at 80 °C overnight. Reactive sintering (synthesis and sintering in the same thermal treatment) was performed using a Field Assisted Sintering Technology/Spark Plasma Sintering (FAST/SPS, FCT-HPD5, FCT Systeme GmbH, Germany). The sintering conditions were heating rate of 20 K/min, maximal temperature of 1200 °C, uniaxial pressure of 30 MPa, dwell time of 15 min, and vacuum (~4 mbar) during the whole thermal cycle. Temperature was controlled using a pyrometer that was focused on the surface of a drilled punch at only 5 mm from the powder. The sintered Cr_2AlC samples were discs of 30 mm diameter and ~ 5 mm thickness, which were ground and polished to eliminate the remaining graphite and prepare the surface.

In order to synthesize the single crystals, we used a flux growth method similar to that described in [17], but using Al_2O_3 instead of graphite crucibles, so as to get a better control of the carbon atomic ratio. Aluminum and chromium pellets were melted in the crucible in an induction-heated growth reactor, with the same atomic ratio as in the Al_8Cr_5 compound. At a temperature of 1650 °C, a carbon rod was actuated through a hole made in the alumina cover, and dipped at a pre-selected depth into the flux, until the dipped part totally dissolved (in around 15mn). The rod was then removed. The final atomic carbon ratio in the flux is around 8%. After carbon dissolution, the flux was cooled down to 1200 °C in one week, and then let to cool down freely. Crystals were extracted from the solidified flux by etching in concentrated HCl.

2.2. Oxidation processes

The polycrystalline and single crystal samples were cut into parallelepipeds ($10 \times 2 \times 2$ mm^3) and triangles, respectively. Both were polished with silicon carbide abrasive disks and finished on felt disk with diamond paste of 0.25 μm particles. The polished samples were placed into a thermogravimetric analysis chamber (TGA, SETARAM EVOSYS-TEM) and heated under argon flow at 20 °C/min. The subsequent isothermal oxidation treatment was performed under dry air flow at T= [800;1500] °C during 100 h.

Additional tests into the thermogravimetric analysis system were carried out on single crystal samples with different surface polishing (4 types of polishing were tested from a silicon carbide disk's grain size of 10–125 μm) in order to evaluate the effect of the surface roughness onto the oxidation behaviour of the sample. The resulting mean roughness was measured by interferometric microscopy (Talysurf CCI 6000, Taylor Hobson). The isothermal oxidation treatment was performed under dry air flow at T=[800;1000] °C during 2 h.

Finally, the long-term oxidation behaviour of polycrystalline samples was investigated. The samples were suspended into a shaft furnace at 1000 °C under ambient air for 1000 h using an alumina rod to avoid contamination of the hanging material.

2.3. Thermodynamic calculations

To support the experimental investigations, thermodynamic analyses of Cr_2AlC equilibrium in air were performed with Thermo-Calc software [18]. The thermodynamic equilibria calculated from this software were based on the CALculation of PHAse Diagrams (CALPHAD) methodology [19]. The relevant thermodynamic descriptions of the Cr-Al-C and CrO_2-Al_2O_3 systems reported, respectively by Y. Liang et al. and by T. M. Besmann et al., were used for the equilibrium calculations of the system [20,21]. The thermodynamic descriptions of the gaseous species considered for the calculations were obtained from the NIST Chemistry WebBook and the work reported by B.B. Ebbinghaus [22,23].

Table 1
Literature main observations on the microstructure of dense bulk Cr_2AlC oxidized at high temperature for a long time.

Ref.	Oxidation temperature (°C)	Time (hours)	Al_2O_3	Cr_7C_3	Porous Cr_7C_3	Cracks	Cr traces	$(Cr,Al)_2O_3$
[4]	1300	336	✓	✓	✓	✓	✓	
[5]	800−1300	20	✓	✓		✓	✓	
[6]	900−1200	480	✓	✓		✓	✓	
[7]	1100−1250	20	✓	✓+Cr_3C_2			✓	
[8]	1000−1300	100	✓	✓	✓	✓		✓
[9]	700−1000	8600	✓	✓			✓	
[10]	900−1200	100	✓				✓	
[11]	1100−1200	100	✓					
[12]	1200	30	✓	✓	✓		✓	

2.4. Microstructural characterization

Scanning electron microscopy (SEM - JEOL 7001-TTLS) and energy dispersive X-Ray spectrometry (EDXS, Oxford Instrument) were used to observe the sample's surface and analyse the composition of the different contrasted regions, before and after oxidation.

X-Ray Diffraction (XRD - BRUKER D8 diffractometer) with Cu-K_α radiation was performed for crystalline structure identification of synthesized and oxidized samples.

3. Results

3.1. Microstructure characterization

Prior to oxidation, the bulk samples are observed and characterized. Fig. 1 shows SEM micrographs in composition mode of the surface of polycrystalline HIP (a), polycrystalline SPS (b), and single crystal (c) Cr_2AlC samples. From image analyses, few quantities Al_2O_3 and Cr_7C_3 impurities are detected into HIP (< 2 %) and SPS (< 4 %) Cr_2AlC samples. Al_2O_3 being inert and Cr_7C_3 an oxidation product, their presence should not affect the oxidation behaviour of the MAX phase. The grain size, revealed after adequate polishing process and polarized optical microscopy image analysis is about 50−100 µm for HIP samples and 2 µm for SPS samples. As a consequence, HIP and SPS samples will be further mentioned as coarse-grained and fine grained samples respectively. The density of the various samples investigated is higher than 98 % of the theoretical density.

Independently of their microstructure, Cr_2AlC samples show several common features after oxidation in the 800−1400 °C temperature range. Indeed, single crystal, coarse and fine grained polycrystal samples exhibit a layered structure composed of the classical α-Al_2O_3 corundum layer and a sublayer of Cr_7C_3, as illustrated in Fig. 2. Pores are also observed in the carbide layer for all types of samples but it isn't systematic nor seems to highly depend on the temperature. Furthermore, depending on the alumina thickness, delamination-induced buckling is observed on the surface of oxidized samples.

In the case of single crystal samples, a significant difference is observed comparing the thickness of alumina formed at the top of the plates and on the sides. The top of the plates, corresponding to an orientation of the basal plane parallel to the surface (Fig. 3-b), formed a thinner oxide scale than the side of the plates, corresponding to an orientation of the basal plane perpendicular to the surface (Fig. 3). It is important here to precise that only the plate faces were polished. Thus, the oxidation of the sides may be affected by the side's roughness.

The short-time oxidation tests performed on single crystal samples with different surface polishing show that the alumina scale thickness increases with introduced roughness for a given oxidation temperature. Indeed, Fig. 4 shows the color change of the alumina with the surface roughness from the synthesis raw material, with its own low intrinsic roughness, to the 1,7 µm deep roughened material for three temperature, 800, 900 and 1000 °C. Such a color change is typical of the alumina scale thickness variation [24] and it demonstrates that the scale thickness can increase by more than 150 % with roughness. From these observations of oxidized single crystal samples, one can deduce that the grain's orientation and roughness of the surface do influence the oxidation process.

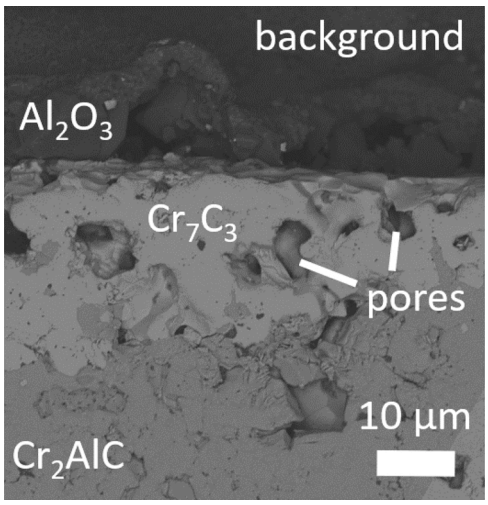

Fig. 2. Cross-sectional SEM micrograph in backscattered mode of an SPS (fine grained) sample oxidized at 1200 °C for 100 h.

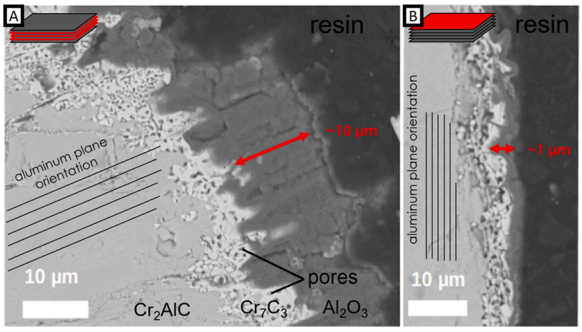

Fig. 3. Cross-sectional SEM micrograph in backscattered mode of the A) side, B) top of the plates of an oxidized single crystal sample at 1200 °C for 2 h.

In the case of the oxidation of a single crystal for 2 h at 1500 °C and for a fine grained polycrystal sample oxidized at 1000 °C for 1000 h, a triple oxide layer is observed with a chromia-rich layer as shown in Fig. 5. EDXS analyses and X-ray maps in Fig. 6 reveal that a mixed aluminum and chromium oxide layer is likely sandwiched in between two alumina layers above the Cr_7C_3 subscale and Cr_2AlC substrate. Three compositions of the oxide are roughly identified. On the top of the surface, the elemental composition is compatible with the presence of alumina. Just below this alumina layer, the elemental composition is compatible with the presence of a chromium rich mixture of oxides (chromia and alumina). Finally, in the vicinity of the internal alumina layer, the elemental composition is compatible with the presence of an aluminum rich mixture of oxides (alumina and chromia).

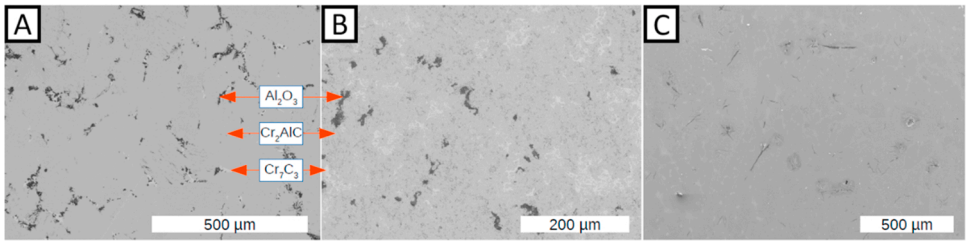

Fig. 1. Surface SEM micrograph in backscattered mode of a) HIP (coarse grained), b) SPS (fine grained), c) single crystal samples.

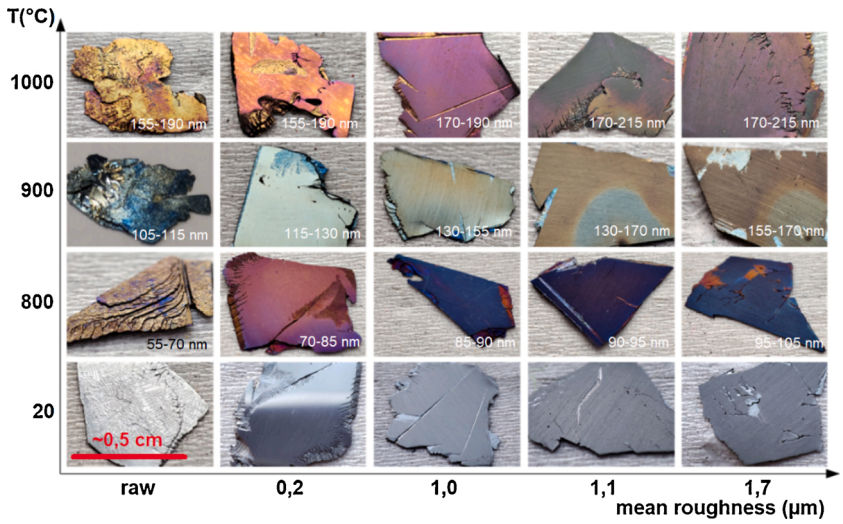

Fig. 4. Photography of single crystal samples with different surface roughness, oxidized for 2 h from 800 to 1000 °C. The estimated thickness of the alumina scale is indicated on each photography [24].

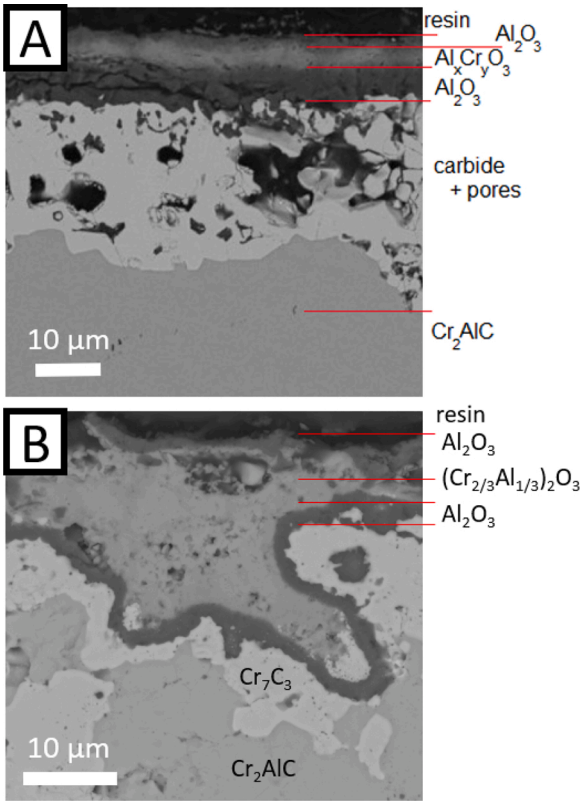

Fig. 5. Cross-sectional SEM micrographs of A) a single crystal sample oxidized at 1500 °C for 2 h; B) a fine-grained sample oxidized at 1000 °C for 1000 h.

3.2. Kinetics

For each sample, the mass gain is measured as a function of time during the oxidation process. The mass gain is thus normalized by the surface of the sample and raised to the power n (integer) until its shape is linear as a function of the oxidation time. One can thus deduce kinetic constant at a given temperature from the slope of the straight line. Most of the mass gain curves could be considered to fit parabolic or cubic law, but we choose to treat our curves using cubic kinetic constant to be able to compare results with recent studies. The kinetic constant can be plotted as a function of 1/T to determine the activation energy of the oxidation mechanism. Fig. 7a shows the mass gain curves obtained during the oxidation of the single crystal. Similar curves are obtained for the fine- and coarse-grained samples. Fig. 7b shows the Arrhenius plots of the cubic kinetic constants determined for the single crystal, fine-grained and coarse-grained polycrystal samples in the temperature range 900−1200 °C.

For the three types of samples, the activation energy is about 400 kJ.mol^{-1}. Such a value is neighbouring the one of 350−380 kJ.mol^{-1} which is the activation energy value for oxygen diffusion at the grain boundaries of alumina [15]. As shown by Smialek et al. for other alumina-forming MAX phases [25], oxygen diffusion at the grain boundaries of the alumina scale is the predominant oxidation mechanism of MAX phases, Cr_2AlC is no exception to this rule.

3.3. CALPHAD calculation

Thermodynamic calculation allows determining which phases are expected to form at the equilibrium. Fig. 8-A shows that four main phases are expected to form as the amount of oxygen in presence with Cr_2AlC increases: aluminum carbide Al_4C_3, two chromium carbides Cr_7C_3 and Cr_3C_2 and an alumina-rich corundum phase (Corundum#1). As the oxygen content continues to increase, a chromia-rich corundum phase (Corundum#2) can also be formed. It is important to note that both of the corundum phases contain alumina and chromia as reported in Fig. 9. The formation of Corundum#2 phase and the increase of Cr_2O_3 in Corundum#1 phase are correlated to the decomposition of the chromium carbides (Fig. 8-A).

However, if a special attention is given to the driving forces of the compound's formation, one can clearly observe in Fig. 8-B and B' that the driving force of the Cr_7C_3 formation is higher than the Cr_3C_2 one. This reveals that the formation of Cr_7C_3 is thermodynamically favoured. More precisely, the order for carbide phases formation is the following: Cr_7C_3 > Cr_3C_2 > Al_4C_3. Considering oxidation temperature above 1300 °C, not represented here for concision considerations, $Cr_{23}C_6$ can be formed with a driving force higher than the aluminum carbide one and below others chromium carbides ones.

Gas species are also formed with mainly CO then CO_2, and very few quantities of chromium oxides. The maximum partial pressures reached by CO and CO_2 are found to be 8.24×10^3 Pa and 6.76×10^3 Pa respectively. Such a result means that the pores of the carbide scale might not be due to chromium evaporation and volatilization. Indeed, the partial pressures of Cr, CrO_2 and Cr_2O_3 in the gas are found lower

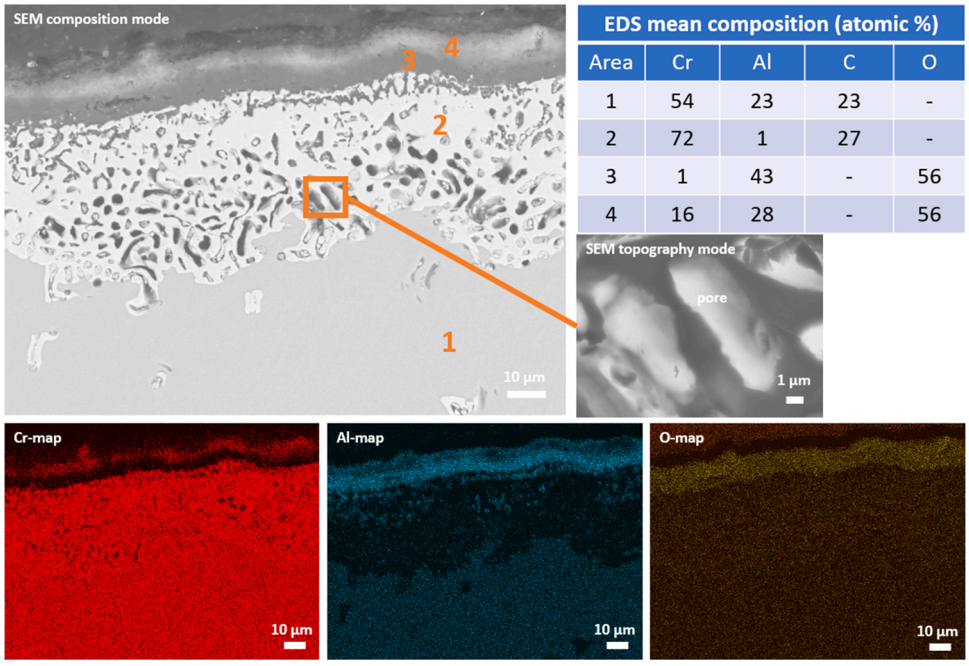

EDS mean composition (atomic %)				
Area	Cr	Al	C	O
1	54	23	23	-
2	72	1	27	-
3	1	43	-	56
4	16	28	-	56

Fig. 6. Cross-sectional SEM micrographs of a single crystal sample oxidized at 1500 °C for 2 h with EDS maps and mean composition of the different areas.

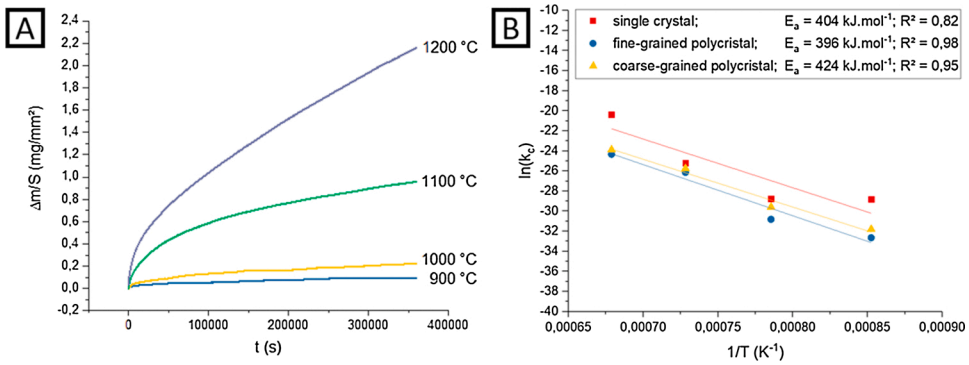

Fig. 7. A) Normalized mass gain curves obtained during oxidation of single crystal's samples and B) Arrhenius plot of the cubic kinetic constant of the single crystal, fine grained, and coarse grained Cr_2AlC samples oxidized in temperature range T=[900–1200] °C.

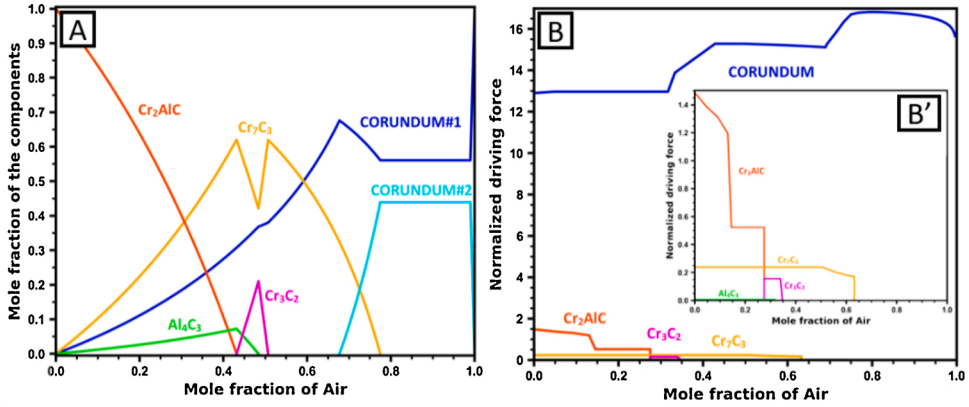

Fig. 8. A) CALPHAD calculations of the mole fraction of compounds at the equilibrium depending on the mole fraction of air. B) CALPHAD calculations of the normalized driving forces of precipitation of the phases depending on the mole fraction of air. B') Zoom.

than 2.25×10^{-2} Pa, 4.5×10^{-5} Pa, 4.4×10^{-3} Pa respectively.

Looking at the proportion of chromia in the most-likely-to-form Corundum#1, calculations show that at low temperature and low mole fraction of air (<0.5), alumina is the only oxide formed. For higher mole fraction of air, alumina is predominant but the proportion of chromia incorporated in the corundum#1 phase increases with

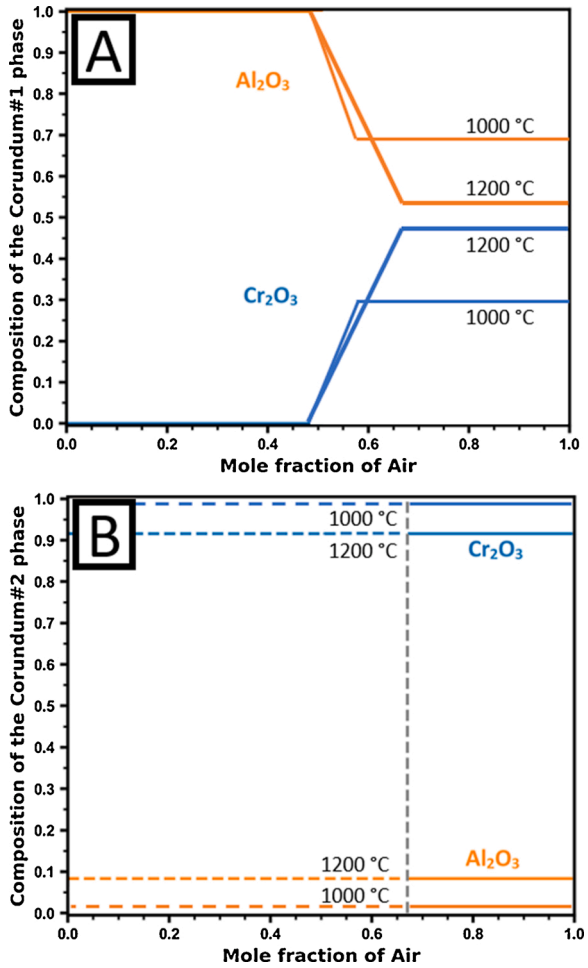

Fig. 9. CALPHAD calculations of the composition of the corundum phases A) Corundum#1, and B) Corundum#2 (dotted lines for metastable phase) at 1000 °C and 1200 °C.

temperature as shown in Fig. 9-A. As shown in Fig. 9-B, a second corundum phase (corundum#2), with a large amount of chromia, is formed for mole fraction of air higher than 0,67.

4. Discussion

Comparing our results to the ones of Table 1, the features of the oxidized samples in this study gather several of the sparse observations in the literature.

The first highlight is about the systematic observation of a Cr_7C_3 subscale under the α-Al_2O_3 scale independently of the oxidation temperature or microstructure. As mentioned in introduction, this feature's explanation is not stated clearly. Thermodynamic calculations via the CALPHAD method performed in this study lead to the conclusion that the driving force of the Cr_7C_3 formation is second next to the alumina's one and is preferred as compared to other carbides ones. We can further advance that absence of carbide or presence of Cr_3C_2 might be due to a non-equilibrium state, kinetics' factors or be proper to thin films since it was mainly observed for thin films [13,14].

It was reported in the literature that the chromium carbide subscale was not observed after long oxidation time of fine-grained samples [11]. This phenomenon was explained as an effect of the large number of grain boundaries providing easy diffusion paths for aluminum atoms, avoiding the Al depletion in the MAX phase grains under the oxide scale. In this study, the observations performed on fine-grained samples seem to belie this statement as one can observe that the grain size, for samples with micrometric grains (2−100 μm), is not the key factor controlling the species formation and the final microstructure. Indeed, in the present study, the carbide layer formed in the oxidized fine-grained, coarse-grained and single crystal samples as well as the thermodynamic calculations strongly suggest that the formation of chromium carbide is inevitable. Moreover, considering the case of aluminum diffusion at grain boundaries, aluminum depletion should be observed in the MAX phase at the vicinity of the interface with the oxide scale which was not reported in the literature nor observed in this study. Worse, it seems that Cr_2AlC has low aluminum depletion tolerance: considering the case of aluminum planes orthogonal to the surface in single crystals, aluminum has a direct path to the surface which should avoid the carbide formation and create aluminum depleted Cr_2Al_xC ($x<1$). Such an hypothesis is disclaimed by our observations. As an explanation for the non-appearance of Cr_7C_3, we therefore suggest that the studied samples in [11] may contain an excess of Al in the grain boundaries due to the synthesis conditions.

The second key point is the fact that the single crystal samples behave similarly to other microstructures. Moreover, the crystallographic orientation of the plates allows observing the orientation's influence on the oxidation process: the oxide scale is thicker in the case of oxide scale formation orthogonal to the basal planes. Also, the oxide scale becomes thicker for high roughness in the case of oxide scale formation parallel to the basal plane, which is equivalent to add basal planes orthogonal to the surface as shown in Fig. 10. These two previous points demonstrate the easy diffusion of the aluminum in the basal plane and match with the well-known self-healing properties of aluminum containing MAX phases [10]. The orientation influence on the oxidation performance is also a common feature of Cr_2AlC with Ti_2AlC and Ti_3AlC_2 MAX phases [26,27].

The last key finding is the chromia-rich corundum scale which is calculated as an equilibrium phase for high oxygen content and is experimentally observed while increasing drastically the oxidation time or temperature. Indeed, increasing oxidation time and/or temperature allows reaching equilibrium state. The multiple-layered system formed can be understood as a consecutive oxidation of the MAX phase and the chromium carbide. Indeed, chromium carbide grains at the interface between Cr_2AlC and the oxide scale of the 1000 h oxidized sample locally showed low carbon content (~10 %), indicating that the chromium carbide does oxidize while the CO_x vaporize. Moreover, the performed thermodynamic calculations explain other studies observations of chromia in the oxide scale [9,10,13]. The singular "sandwiched" position of the chromia-rich corundum in the scale remains unexplained: after formation of the alumina scale, whether the chromium from the chromium carbide diffused outward and stabilized in the alumina corundum, or the chromium carbide sublayer oxidized into chromia and allowed inward diffusion of the oxygen and further oxidation of the MAX phase into Al_2O_3.

Another interesting feature common to several samples is the presence of pores in the chromium carbide layer. These pores were previously explained by carbon oxide or chromia evaporation [6–9]. The thermodynamic calculations indicate a very low proportion of chromium-based gas species but significative carbon oxides gas species. Therefore, the presence of pores can be partially explained by the carbon oxides volatilization. Indeed, thermodynamic calculations allows demonstrating that CO and CO_2 gases are produced during oxidation. Moreover, CO_2 is experimentally detected by Lin et al. [5]. Considering the pores proportion in the Cr_7C_3 layer observed in Figs. 2 or 3, one can expect that it's only part of the explanation. Diffusion coefficient of chromium in the alumina layer is likely very small due to the long time or high temperature necessary to observe the chromia rate increase in the corundum scale. Therefore, the difference between the slow diffusion of chromium compared to the fast one of aluminum in the structure could create vacancies which further segregate to form Kirkendall voids. The carbon volatilization and the creation of Kirkendall voids during the oxidation thus likely explain the observed porosity.

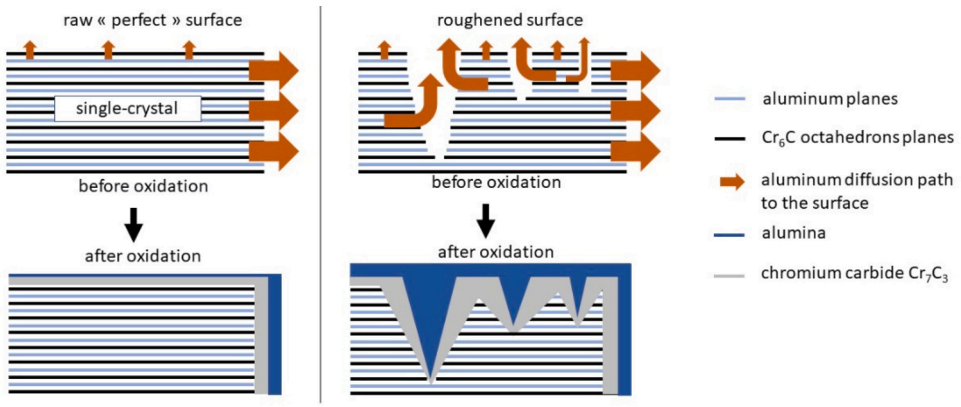

Fig. 10. Schematic illustration (not to scale) of roughness and orientation influence on the oxidation of Cr_2AlC single crystal.

5. Conclusion

Oxidation tests were carried out on bulk single crystal and on fine and coarse grained polycrystal samples in the temperature range 800−1500 °C for up to 1000 h. Thermodynamic calculations were also performed to give further analysis of the experiments. Single crystal, fine grained and coarse grained polycrystals behave similarly despite different microstructures: a continuous alumina layer and a chromium carbide Cr_7C_3 sublayer are formed on the surface of Cr_2AlC. Calculation of the driving forces of phase formation justifies the preferential formation of Cr_7C_3 as compared to other chromium carbides. Cross-sectional observations of specific region and introduction of roughness on the single crystal's surface allow demonstrating that grain orientation and roughness does influence the alumina thickness. These results are a consequence of the high mobility of alumina atoms in the basal plane of the MAX phase.

Increasing time or temperature results in the formation of more and more chromia in the alumina-rich corundum. For high enough temperature or oxidation duration, a chromia-rich corundum phase is formed instead of the alumina-rich corundum phase. Such a result is in very good agreement with thermodynamic calculations. The successful match between the thermodynamic calculations and experimental data show the importance of long-time oxidation experiments and driving force calculations for the understanding of the oxidation processes.

Declaration of Competing Interest

The authors declare that they have no known competing financial interests or personal relationships that could have appeared to influence the work reported in this paper.

Acknowledgements

Special thanks to the Région Nouvelle-Aquitaine and the Ministère de l'Enseignement Supérieur et de la Recherche for funding this research. This work was supported by the French government program "Investissements d'Avenir" (EUR INTREE, reference ANR-18-EURE-0010). This work was supported by the European commission through the Horizon 2020 project IL TROVATORE (n° 740415).

References

[1] M.W. Barsoum, The $M_{n+1}AX_n$phases: a new class of solids: thermodynamically stable nanolaminates, Prog. Solid State Chem. 28 (2000) 201–281, https://doi.org/10.1016/S0079-6786(00)00006-6.

[2] M. Sokol, V. Natu, S. Kota, M.W. Barsoum, On the chemical diversity of the max phases, Trends Analyt. Chem. 1 (2019) 210–223, https://doi.org/10.1016/j.trechm.2019.02.016.

[3] D.J. Tallman, J. Yang, L. Pan, B. Anasori, M.W. Barsoum, A critical review of the oxidation of Ti_2AlC, Ti_3AlC_2 and Cr_2AlC in air, Mater. Res. Lett. 1 (2013) 115–125, https://doi.org/10.1080/21663831.2013.806364.

[4] D.B. Lee, T.D. Nguyen, J.H. Han, S.W. Park, Oxidation of Cr_2AlC at 1300 °C in air, Corros. Sci. 49 (2007) 3926–3934, https://doi.org/10.1080/21663831.2013.806364.

[5] Z.J. Lin, M.S. Li, J.Y. Wang, Y.C. Zhou, High-temperature oxidation and hot corrosion of Cr_2AlC, Acta Mater. 55 (2007) 6182–6191, https://doi.org/10.1016/j.actamat.2007.07.024.

[6] D.B. Lee, S.W. Park, Oxidation of Cr_2AlC between 900 and 1200 °C in air, Oxid. Met. 68 (2007) 211–222, https://doi.org/10.1007/s11085-007-9071-0.

[7] W. Tian, P. Wang, Y. Kan, G. Zhang, Oxidation behavior of Cr_2AlC ceramics at 1,100 and 1,250 °C, J. Mater. Sci. 43 (2008) 2785–2791, https://doi.org/10.1007/s10853-008-2516-2.

[8] D.B. Lee, T.D. Nguyen, Cyclic oxidation of Cr_2AlC between 1000 and 1300 °C in air, J. Alloys. Compd. 464 (2008) 434–439, https://doi.org/10.1016/j.jallcom.2007.10.018.

[9] D.B. Lee, T.D. Nguyen, S.W. Park, Long-time oxidation of Cr_2AlC between 700 and 1,000 °C in air, Oxid. Met. 77 (2012) 275–287, https://doi.org/10.1007/s11085-012-9285-7.

[10] S. Li, L. Xia, G. Song, X. Wu, W.G. Sloof, S. van der Zwaag, Oxidation and crack healing behavior of a fine-grained Cr_2AlC ceramic, J. Am. Ceram. Soc. 96 (2013) 892–899, https://doi.org/10.1111/jace.12170.

[11] S. Li, X. Chen, Y. Zhou, G. Song, Influence of grain size on high temperature oxidation behavior of Cr_2AlC ceramics, Ceram. Int. 39 (2013) 2715–2721, https://doi.org/10.1016/j.ceramint.2012.09.039.

[12] J. Gonzalez-Julian, T. Go, D.E. Mack, R. Vaßen, Environmental resistance of Cr2AlC MAX phase under thermal gradient loading using a burner rig, J. Am. Ceram. Soc. 101 (2018) 1841–1846, https://doi.org/10.1111/jace.15425.

[13] D.E. Hajas, M. to Baben, B. Hallstedt, R. Iskandar, J. Mayer, J.M. Schneider, Oxidation of Cr_2AlC coatings in the temperature range of 1230 to 1410 °C, Surf. Coat. Technol. 206 (2011) 591–598, https://doi.org/10.1016/j.surfcoat.2011.03.086.

[14] Z. Wang, G. Ma, L. Liu, L. Wang, P. Ke, Q. Xue, Aiying Wang, High-performance Cr_2AlC max phase coatings: Oxidation mechanisms in the 900–1100 °C temperature range, Corros. Sci. 167 (2020), 108492, https://doi.org/10.1016/j.corsci.2020.108492.

[15] J.L. Smialek, Oxygen diffusivity in alumina scales grown on Al-MAX phases, Corros. Sci. 91 (2015) 281–286, https://doi.org/10.1016/j.corsci.2014.11.030.

[16] M. Venkatraman, J.P. Neumann, The C-Cr (carbon-chromium) system, Bull. Alloy. Phase Diagr. 11 (1990) 152–159, https://doi.org/10.1007/BF02841701.

[17] T. Ouisse, E. Sarigiannidou, O. Chaix-Pluchery, H. Roussel, B. Doisneau, D. Chaussende, High temperature solution growth and characterization of Cr_2AlC single crystals, J. Cryst. Growth 384 (2013) 88–95, https://doi.org/10.1016/j.jcrysgro.2013.09.021.

[18] J.-O. Andersson, T. Helander, L. Höglund, P. Shi, B. Sundman, Thermo-calc and dictra, CALPHAD 26 (2002) 273–312, https://doi.org/10.1016/S0364-5916(02)00037-8.

[19] B. Sundman, H.L. Lukas, S.G. Fries, Computational Thermodynamics: the Calphad Method, Cambridge University Press, 2007.

[20] B. Hallstedt, D. Music, Z. Sun, Thermodynamic evaluation of the Al-Cr-C system, Zeitschrift für Metallkunde 97 (2006) 539–542, https://doi.org/10.3139/146.101270.

[21] T.M. Besmann, N.S. Kulkarni, K.E. Spear, Thermochemical analysis and modelling of the Al_2O_3 - Cr_2O_3, Cr_2O_3 -SiO_2, and Al_2O_3 -Cr_2O_3 -SiO_2 systems relevant to refractories, J. Am. Ceram. Soc. 89 (2006) 638–644, https://doi.org/10.1111/j.1551-2916.2005.00719.x.

[22] P.J. Linstrom, W.G. Mallard, NIST Chemistry Webbook, NIST Standard Reference Database 69 [data Set], National Institute of Standards and Technology, 1997.

[23] B.B. Ebbinghaus, Thermodynamics of gas phase chromium species: the chromium oxides, the chromium oxyhydroxides, and volatility calculations in waste incineration processes, Combust. Flame 93 (1993) 119–137, https://doi.org/10.1016/0010-2180(93)90087-J.

[24] Sampuran-Singh, K.V. Anand, Electrochemical properties of dielectric films of aluminium oxide deposited on silicon, Thin Solid Films 37 (1976) 453–460, https://doi.org/10.1016/0040-6090(76)90613-1.
[25] J.L. Smialek, Kinetic aspects of Ti_2AlC max phase oxidation, Oxid. Met. 83 (2015) 351–366, https://doi.org/10.1007/s11085-015-9526-7.
[26] E. Drouelle, V. Gauthier-Brunet, J. Cormier, P. Villechaise, P. Sallot, F. Naimi, F. Bernard, S. Dubois, Microstructure-oxidation resistance relationship in Ti_3AlC_2 MAX phase, J. Alloys. Compd. 826 (2020), https://doi.org/10.1016/j.jallcom.2020.154062.
[27] X. Li, X. Xie, J. Gonzalez-Julian, J. Malzbender, R. Yang, Mechanical and oxidation behavior of textured Ti_2AlC and Ti_3AlC_2 MAX phase materials, J. Eur. Ceram. Soc. 40 (2020) 5258–5271, https://doi.org/10.1016/j.jeurceramsoc.2020.07.043.